Spallation of ^{32}S ions at ultra-relativistic energies in nuclear emulsion

M. El-Nadi, A. Abdelsalam, E.A. Shaat, N. Ali Mossa, Z. Abou Moussa, S. Kamel, N. Rashed, W. Osman, and M.E. Hafiz

Abstract: Partial production cross sections of electromagnetic breakup of ^{32}S projectiles at two widely differing energies were measured using an emulsion target. The electromagnetic dissociation represents about 6% and 17% of the total number of nuclear events at $E_{lab}/A = 3.7$ and 200 GeV, respectively. The experimental electromagnetic cross sections σ_{EMD}^{exp} show an energy dependence that is well reproduced by the Weizsäcker–Williams approximation. The value of σ_{EMD}^{exp} at 200A GeV (with $\gamma \gg 1$) shows a good agreement with that predicted by the combined model of Pshenichnov et al. Examination of the reactions (γ, p) and (γ, He) reveals that the ratio of 1 p/1 He cross sections is close to unity at Dubna energy (3.7A GeV), while it rapidly increases to 3.0 ± 0.6 at CERN energy (200A GeV). In most of the observed dissociation modes, the total kinetic energy of the fragments in the projectile rest frame is lower than 50 MeV. Nevertheless, it is possible that the contribution of excitation modes of the different multipolarities is determining in this region.

PACS No.: 25.70

Résumé : Utilisant une cible en émulsion, nous mesurons les sections efficaces partielles de production dans la cassure électromagnétique du projectile ^{32}S à deux énergies très différentes. La dissociation électromagnétique représente approximativement 6 % et 17 % du nombre total d'événements nucléaires à $E_{lab}/A = 3.7$ et 200 GeV respectivement. La section efficace électromagnétique expérimentale, σ_{EMD}^{exp} montre une dépendance en énergie qui est bien décrite par l'approximation de Weizsäcker-Williams. La valeur de σ_{EMD}^{exp} à 200A GeV (avec $\gamma \gg 1$) est en bon accord avec celle prédite par le modèle combiné de Pshenichnov et al. L'examen des réactions (γ, p) et (γ, He) montre que le rapport 1p / 1He est près de l'unité aux énergies de Dubna (3,7A GeV), alors qu'il augmente rapidement à 3,0 ± 0,6 au CERN (200A GeV). Dans la plupart des modes de dissociation observés, l'énergie cinétique totale des fragments dans le référentiel du projectile au repos est plus petite que 50 MeV. Il est néanmoins possible que les contributions des modes d'excitation soit dominantes dans cette région.

[Traduit par la Rédaction]

Received 19 March 2002. Accepted 15 November 2003. Published on the NRC Research Press Web site at http://cjp.nrc.ca/ on 12 May 2004.

M. El-Nadi,[1] **A. Abdelsalam, E.A. Shaat, Z. Abou Moussa, and W. Osman.** Physics Department, Faculty of Science, Cairo University, Giza, Egypt.
N. Ali Mossa. Basic Science Department, Faculty of Engineering, Banha Branch, Zagazig University, Egypt.
S. Kamel[2] **and M.E. Hafiz.** Physics Department, Faculty of Education, Ain Shams University, Cairo, Egypt.
N. Rashed. Physics Department, Faculty of Science, Cairo University, Fayoum Branch, Fayoum, Egypt.

[1] Deceased.
[2] Corresponding author (e-mail: sayedks@hotmail.com).

 doi: 10.1139/P03-125

1. Introduction

The recent experiments on relativistic heavy ion (RHI) collisions indicate the importance of studying nuclear matter under extreme conditions. In central nucleus–nucleus interactions, RHI collisions are used to study the properties of compressed and heated nuclear matter, and in addition offer the possibility of observing the signatures of an unusual form of matter, such as quark–gluon plasma. On the other hand, very strong electromagnetic fields are present for a very short time in "distant" collisions [1] with no nuclear contact. Such fields can lead to a large probability for the excitation of giant resonances in extreme peripheral collisions. Since the giant resonances mainly decay by particle emission, this process makes an appreciable contribution to the fragmentation of the nuclei. Few groups have studied experimentally the dissociation of RHI using nuclear emulsion [2–8] in distant electromagnetic collisions, i.e., in those with impact parameters larger than $R_T + R_P$ (the sum of the respective radii of target and projectile nuclei). Generally, since emulsion has better spatial resolution than any other detector, the emulsion technique becomes very important. This is especially the case at ultrarelativistic energies, where the opening angles of the projectile fragments are very narrow. Despite the heterogeneity of the emulsion target, it can be successfully used to measure the electromagnetic dissociation (EMD) cross section.

The first attempt to study the EMD of projectiles using nuclear emulsion was reported by Ardito et al. [2]. These workers used ^{16}O projectiles at CERN energies (60A and 200A GeV). They found that the electromagnetic effects increase with the projectile energy as well as with Z_T^2, where Z_T is the charge of the target nucleus, with the main contributors in the emulsion being the silver ($Z_T = 47$) and bromine ($Z_T = 35$) nuclei. Afterwards, Singh and co-workers [3, 4] reported that at 200A GeV the production cross section of EMD for projectiles increases by $\sim 2.5\times$ when the projectile charge is doubled from $Z_P = 8$ to $Z_P = 16$. This result was also reported by Baroni et al. [5], who studied the exclusive channels involving charged fragments as a function of the energy released in the interaction. The latter point is of interest in this work. Bahk et al. [6] investigated the EMD of 14.5A GeV ^{28}Si at the Brookhaven National Laboratory (BNL) Alternating Gradient Synchrotron (AGS). Singh and Jain [4] studied the EMD of the same projectile with much higher statistics and found that the majority of the events in the most prominent decay modes ($^{28}\mathrm{Si} \rightarrow {}^{27}\mathrm{Al}+\mathrm{p}$) can be attributed to the excitation of Giant Dipole Resonances (GDRs). Recent experimental work [7, 8] in nuclear emulsion has concentrated on the projectile multifragment breakup of light ions (such as ^{6}Li, ^{12}C, and ^{16}O) at Dubna energy (3.7A GeV) using the Weizsäcker–Williams (WW) method [9], confirming the dependence of the EMD cross section on the projectile charge and energy. Moreover, in the multiplicity distribution of He fragments, the majority of EMD events in such studies lie in the channels producing single He fragments (see Sect. 4).

Very recently, as reported in ref. 10*a*, we extended the EMD study of light ions at the Dubna energy reported in refs. 7 and 8 to include ^{32}S ions. We found the single-alpha emission through the $^{32}\mathrm{S}(\gamma, \mathrm{He})^{28}\mathrm{Si}$ channel to be the dominant process at 3.7A GeV. Reference 10 also includes a study of the EMD detected for the 200A GeV ^{32}S projectile. In this case the dominant channel was found to be the emission of a proton through the $^{32}\mathrm{S}(\gamma, \mathrm{p})^{31}\mathrm{P}$ channel. It thus becomes possible to compare the effective role of the different reaction mechanisms (Coulomb and peripheral nuclear interactions) induced by ^{32}S ions at these two widely differing energies. The measurements of the excitation energy spectrum [11] in relativistic collisions between heavy ions can produce information of value in understanding the nuclear structure and in searching for structures excited by higher order processes. The present work is an extension of our previous investigation [10*a*]. Here we focus on the excitation energy distributions for the observed decay channels at 200A GeV ^{32}S, in addition to comparing these distributions with those measured by Baroni et al. [5]. In the present paper, the exclusive cross sections for the detected decay channels of EMD for both 3.7A and 200A GeV ^{32}S ions are analyzed as well.

Table 1. The chemical compositions of the Br-2 and Fuji nuclear emulsions used for 3.7*A* and 200*A* GeV, respectively.

	(No. of atoms/cm^3) $\times 10^{22}$	
Element	Br-2	Fuji
H	3.150	3.2093
C	1.412	1.3799
N	0.395	0.3154
O	0.956	0.9462
S	—	0.0134
I	—	0.00552
Br	1.031	1.0034
Ag	1.036	1.0093

Table 2. Topologies of the interactions of projectiles with nuclear emulsions at various energies.

Projectile	Energy/*A* (GeV)	Track length (cm)	N_{nuc}	N_{EMD}	$R\%$	Lorentz factor γ	$E_\gamma^{\max}$ (MeV)	Ref.
^{6}Li	3.7	150.00	968	70	7.20 ± 0.86	4.51	99.40	8
^{12}C	3.7	144.00	1000	21	2.10 ± 0.46	4.51	100.50	7
^{16}O	3.7	86.20	708	45	6.35 ± 0.94	4.51	98.10	8
^{32}S	3.7	74.50	780	47	6.02 ± 0.88	4.51	103.70	This work
^{28}Si	14.5	174.90	1408	109	7.74 ± 0.74	15.57	288.50	4
^{16}O	60	16.40	131	9	6.87 ± 2.30	64.41	1392.30	2
^{16}O	200	348.70	2934	362	12.34 ± 0.65	214.71	4641	5
^{32}S	200	112.60	1249	210	16.81 ± 1.16	214.71	3955	This work
^{32}S	200	198.50	2168	476	21.96 ± 1.01	214.71	3955	5
^{32}S	200	127.40	1157	197	17.03 ± 1.21	214.71	3955	3

2. Predictions for EMD at Dubna and CERN energies

Electromagnetic processes at relativistic and ultrarelativistic energies can be treated accurately with the equivalent photon method [1, 9]. In this method, the cross section of EMD for a projectile of mass A_{P} can be calculated as

$$\sigma_{\text{EMD}} = \int N(E_\gamma)\, \sigma_{A_{\text{P}}}(E_\gamma)\, \mathrm{d}E_\gamma$$

where $\sigma_{A_{\text{P}}}(E_\gamma)$ is the measured photoabsorption cross section [12] and $N(E_\gamma)$ is the virtual photon flux obtained by integration over impact parameters $b > b_{\min}$. This restriction leads to a rough upper limit $E_\gamma^{\max}$ of the energies in the virtual photon spectrum and hence on the excitation energies, which can be reached by electromagnetic processes. The value of $E_\gamma^{\max}$ is approximately given [1] by

$$E_\gamma^{\max} = \frac{\hbar c \gamma_{\text{P}}}{b_{\min}}$$

where $\hbar c \approx 197$ nm eV, γ_{P} is the Lorentz boost parameter of the projectile motion relative to the target nucleus, and $b_{\min} (= R_{\text{P}} + R_{\text{T}})$ is the minimum impact parameter below which nuclear processes dominate over electromagnetic ones.

Values, as estimated according to this method, of γ_{P} and $E_\gamma^{\max}$ for an Ag target nucleus (the heaviest and most abundant element in the emulsion [13]; see Table 1) using different projectiles at different

Fig. 1. Virtual photon spectra expected at different energies for different incident projectiles on Ag target nucleus.

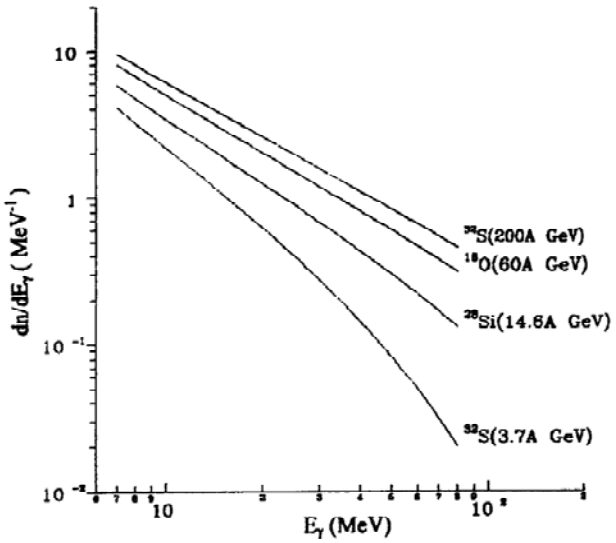

energies are listed in Table 2. Also, the virtual photon spectra expected, respectively, for ^{32}S, ^{28}Si, and ^{16}O projectiles at 3.7A and 200A, 14.5A, and 60A GeV are shown in Fig. 1. Our conclusion, similar to the results of ref. 14, is that the photon spectrum hardens with increasing incident energy, because of the increasing Lorentz contraction of the field as seen by the projectile. For the present work, at 3.7A GeV ($\gamma_P \approx 4.5$), $E_\gamma^{max} \approx 100$ MeV, which is less than the pion production threshold. On the other hand, at 200A GeV ($\gamma_P \approx 215$), $E_\gamma^{max} \approx 4$ GeV, which could produce a $\Delta(1232)$ resonance. This Δ resonance would subsequently dissociate into a nucleon and a pion, either of which can initiate a two-step process of intranuclear cascade. The present results for ^{32}S at the two energies used ensure that no pions are associated with the pure EMD events. The experimental absence of pions is theoretically confirmed in Fig. 2, obtained at an energy of 200A GeV by Pshenichnov et al. [15] using the Monte Carlo technique. This technique simulates the energy E_γ of a virtual photon distributed according to the product $N(E_\gamma)\,\sigma_{A_P}(E_\gamma)$, which is proportional to the probability of the electromagnetic interaction. In fact, the nature of a photonuclear interaction depends on the energy of the incident photon, with the projectile nucleus absorbing photons by GDRs at $E_\gamma < 40$ MeV, by a quasi-deuteron effect at $40 \leq E_\gamma \leq 140$ MeV, and by photoproduction of hadrons at higher energy ($E_\gamma > 140$ MeV). However, whereas soft photons (those with energy $E_\gamma \leq 100$ MeV) dominate the virtual photon spectrum of Fig. 2, a realistic prediction of σ_{EMD} at 200A GeV would ascribe the interaction mainly to the GDR and quasi-deuteron regimes, with $E_\gamma \leq 140$ MeV.

3. Experimental technique

The experimental procedure used in the present research is very similar to the one discussed extensively in the work of Baroni et al. [5]. Here, two stacks of nuclear emulsions were exposed horizontally to ^{32}S ion beams, but at two widely differing energies. The first stack, consisting of Br-2 emulsion pellicles, was irradiated by 3.7A GeV ^{32}S ions at the Dubna Synchrophasotron. The second, consisting of Fuji films, was exposed to 200A GeV ^{32}S at the CERN Super Proton Synchrotron (SPS) (Exp. No.

Fig. 2. Product $N(E_\gamma)\sigma_{A_p}(E_\gamma)$ as a function of the virtual photon energy E_γ.

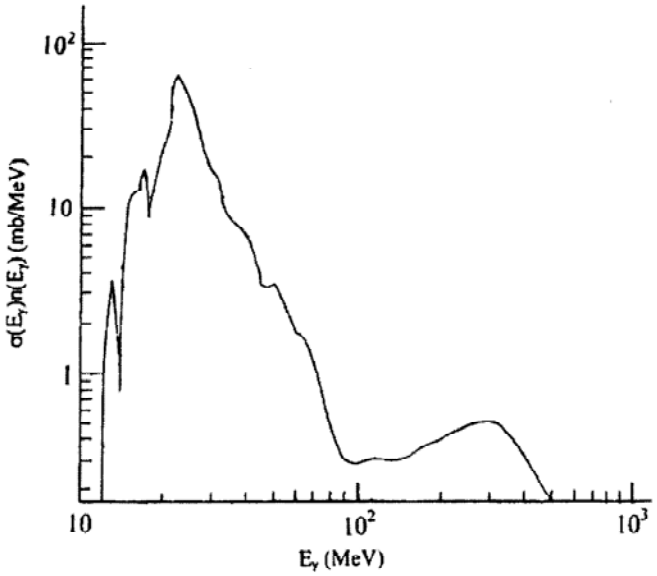

EMU03). The compositions of the two stacks used are presented in Table 1. The pellicles were scanned under 100× magnification with an "along-the-track" technique, with our beam tracks picked up at 4 mm from the entrance edge and within the central 80% of the pellicle thickness. Each beam track was carefully followed up to a distance of 5 cm or until the point of interaction with an emulsion nucleus. Other details concerning irradiations and scanning are given in refs. 16–18. In this work, we followed total track lengths of 75.0 and 112.6 m, corresponding to 3.7A and 200A GeV ^{32}S, and observed 832 and 1459 interactions, respectively. The corresponding total interaction mean-free-path lengths λ_{tot} are 9.01 ± 0.31 cm and 7.72 ± 0.20 cm, respectively. Interactions were analyzed by studying the tracks emitted from each interaction detected. These tracks were classified according to the commonly accepted emulsion-experiment terminology, based upon their ionization and measured properties, following refs. 16 and 17.

Pure nuclear fragmentation [16, 17] and electromagnetic dissociation [10, 18] events for the two energies used were detected. The pure nuclear fragmentation events are associated with the production of target fragments (mostly protons of kinetic energy $E < 40$ MeV, recoil protons in the kinetic-energy range $40 < E < 400$ MeV, and relativistic created pions) as well as projectile fragments (PFs) emitted in a forward narrow cone. The present candidate EMD events (extremely peripheral interactions) were selected with the condition that there be no visible target excitation or secondary particle production, together with the condition that the sum of measured charges of all the PFs with ($Z \geq 1$) inside the fragmentation cone must equal the charge of the incident beam. This narrow fragmentation forward cone is defined [17] by vertex angle $\theta = 44$ mrad for 3.7A GeV and 1 mrad for 200A GeV. Upon application of these stringent selection criteria, the numbers of clean EMD events corresponding to the ^{32}S projectile at 3.7A and 200A GeV were found to be 47 and 210, respectively. Charge measurements were performed on projectile EMD fragments by δ-ray counting. For light fragments ($Z = 2$–4), complementary gap counting was undertaken [19]. The space angles of all PFs in EMD events at 200A GeV were determined from the vector directions of the incident beam and emitted fragments following ref. 3. The accuracy in the angular measurements in the emulsion is higher than 0.1 mrad for angles $\theta \leq 1$ mrad.

Table 3. Nuclear and EMD mean-free-path lengths (λ_{nuc} and λ_{EMD}) and cross sections ($\sigma_{NUC} = 1/n_{em}\lambda_{NUC}$ and $\sigma_{EMD} = f/\rho\lambda_{EMD}$, where f is the weight factor for the Ag target component in the emulsion).

Projectile	Energy/A (GeV)	λ_{nuc} (cm)	λ_{EMD} (cm)	σ_{nuc} (mb)	f	σ_{EMD} (mb)	Ref.
^{6}Li	3.7	15.50 ± 0.55	214.30 ± 25.6	1131.9 ± 40.2	0.61	304.1 ± 36.3	8
^{12}C	3.7	14.40 ± 0.33	685.70 ± 149.6	879.3 ± 20.1	0.61	86.5 ± 18.9	7
^{16}O	3.7	12.18 ± 0.33	191.60 ± 28.6	1039.5 ± 28.2	0.67	340.2 ± 50.8	8
^{32}S	3.7	9.55 ± 0.34	158.50 ± 23.1	1313.9 ± 47.2	0.62	387.3 ± 56.4	This work
^{16}O	14.5	13.42 ± 0.60	216.00 ± 39.9	943.5 ± 42.2	0.62	284.2 ± 52.5	6
^{28}Si	14.5	12.42 ± 0.33	160.50 ± 15.4	1019.0 ± 27.0	0.62	383.0 ± 37.0	4
^{28}Si	14.5	10.37 ± 0.39	155.90 ± 22.9	1221.0 ± 46.0	0.62	394.0 ± 58.0	6
^{16}O	60	12.50 ± 1.10	117.00 ± 31.0	1012.9 ± 89.1	0.61	516.2 ± 138.6	2
^{16}O	200	12.25 ± 0.40	103.70 ± 9.8	1033.0 ± 38.0	0.62	592.0 ± 57.0	4
^{16}O	200	11.73 ± 0.48	101.90 ± 12.4	1079.0 ± 44.0	0.61	602.0 ± 73.0	6
^{16}O	200	11.88 ± 0.22	96.30 ± 5.1	1066.0 ± 20.0	0.62	670.0 ± 35.0	5
^{32}S	200	9.02 ± 0.25	40.10 ± 2.7	1406.9 ± 39.0	0.62	1530.8 ± 103.1	This work
^{32}S	200	9.16 ± 0.20	42.20 ± 2.0	1382.3 ± 30.2	0.61	1680.0 ± 80.0	5
^{32}S	200	11.01 ± 0.32	42.00 ± 2.0	1150.0 ± 34.0	0.61	1438.0 ± 68.5	3

4. Results

The topologies of the inelastic and electromagnetic interactions observed in the present ^{32}S–emulsion interactions at 3.7A and 200A GeV are displayed in Table 2. For comparison, the results obtained by other authors for assorted projectiles and energies are tabulated also. Table 2 indicates that apart from 3.7A GeV ^{12}C, the value in the energy range from 3.7A up to 60A GeV of R%, the ratio (expressed as a percentage) of the number of EMD events (N_{EMD}) to that of nuclear events (N_{nuc}) is nearly independent both of the projectile's energy and of its mass. (In this energy range, R% maintains a value around 6%.) On the other hand, as the energy increases to 200A GeV, the value of R% increases with the mass number of the projectile. However, it can be observed that the effect of projectile energy on the EMD process is significantly larger than the effect of projectile mass: for ^{32}S, R% increases from ≈6% at 3.7A GeV to ≈ 16.8% at 200A GeV, whereas at 200A GeV, $R\% \approx 12.3\%$ and 16.8% for ^{16}O and ^{32}S, respectively. These observations are expected, since while the nuclear interaction cross section is approximately constant with energy (limiting the fragmentation), that of the EMD should significantly increase at 200A GeV because of the much stronger virtual-photon cross section. These results are in qualitative agreement with the predictions of virtual-photon theory [1, 9] at the highest energy used (with $\gamma \gg 1$). Despite the low statistics for ^{32}S events at 3.7A GeV, the resulting R% (≈6%) is in fair agreement with the corresponding value reported in ref. 20 from a solid-state nuclear track detector. Our result for 200A GeV ^{32}S is also found to be in reasonable agreement with that of refs. 3 and 5. It should be taken into account that with emulsions it is impossible to observe neutron emission or to distinguish between various isotopes. Therefore, the mean-free-path lengths λ_{EMD} for the overall EMD processes at 200A GeV listed in Table 3 are corrected for the undetected disintegration modes ^{31}S + n, ^{30}S + 2n, and so on, following refs. 2 and 3. Table 3 displays our experimental data for λ_{nuc} and λ_{EMD} in comparison with values obtained by other authors for assorted projectiles at various different energies. Our results fit into the trends in the tabulated data.

It is known that nuclear emulsion is a heterogeneous target. Therefore, to evaluate the absolute value of the cross section σ_{EMD} for EMD, and also to compare the present results with those of other experiments on a single target [12, 20, 21] or an emulsion target [3, 5], the parameter λ_{EMD} in emulsion should be converted into an absolute cross section on a silver (Ag) target, the heaviest abundant con-

Table 4. Production cross section for the overall EMD process and partial cross sections in different decay modes for ^{32}S at 3.7A and 200A GeV. The data for the highest energy are compared with those of ref. 3.

	Cross section (mb)		
	3.7A GeV ^{32}S	200A GeV ^{32}S	
Decay mode	This work	This work	Ref. 3
Overall EMD process	387.3 ± 56.4	1530.8 ± 103.1	1438.0 ± 80.0
P + p	107.1 ± 29.7	501.5 ± 52.3	341.4 ± 40.2
Si + He	131.9 ± 33.0	163.5 ± 29.9	118.5 ± 23.7
Si + 2p	32.9 ± 16.6	109.0 ± 24.4	123.3 ± 24.2
Al + He + p	32.9 ± 16.6	81.8 ± 21.1	47.4 ± 15.0
Al + 3p	—	32.7 ± 13.4	47.4 ± 15.0
Mg + 2He	—	27.3 ± 12.2	4.7 ± 4.7
Mg + He + 2p	24.7 ± 14.3	21.8 ± 10.9	61.6 ± 17.1
Mg + 4p	16.5 ± 11.7	27.3 ± 12.2	4.7 ± 4.7
Na + 2He + p	—	21.8 ± 10.9	4.7 ± 4.7
Na + Li + 2p	—	5.5 ± 5.5	9.5 ± 6.7
Na + He + 3p	—	21.8 ± 10.9	4.7 ± 4.7
Na + 5p	—	16.4 ± 9.4	—
Ne + 2He + 2p	16.5 ± 11.7	16.4 ± 9.4	9.5 ± 6.7
Ne + He + 4p	—	16.4 ± 9.4	4.7 ± 4.7
F+2He+3p	—	5.5 ± 5.5	14.2 ± 8.2
F+3He+p	—	11.1 ± 7.9	9.5 ± 6.7
O + 3He + 2p	—	5.5 ± 5.5	—
O + 2He + 4p	—	5.5 ± 5.5	14.2 ± 8.2
N + 3He + 3p	—	5.5 ± 5.5	9.5 ± 6.7
N + 2He + 5p	—	5.5 ± 5.5	4.7 ± 4.7
2C + 2He	8.3 ± 8.3	—	—
2C + 3He + 4p	—	5.5 ± 5.5	4.7 ± 4.7
B + 4He + 3p	—	5.5 ± 5.5	—
B + 2He + 7p	—	5.5 ± 5.5	4.7 ± 4.7
Be + 2He + 8p	—	5.5 ± 5.5	—
Be + 3He + 6p	8.3 ± 8.3	—	—
Li + 5He + 3p	8.3 ± 8.3	—	—
Li + 4He + 5p	—	5.5 ± 5.5	—
6He + 4p	—	5.5 ± 5.5	—
5He + 6p	—	5.5 ± 5.5	4.7 ± 4.7
4He + 8p	—	5.5 ± 5.5	—

stituent of the emulsions. The presence of iodine and sulphur, whose abundances in nuclear emulsion are very small, is neglected. Following ref. 4, the total production cross section for EMD events due to the Ag target corrected for neutron channels is computed from the relation $\sigma_{EMD} = f/\rho\,\lambda_{EMD}$, where ρ is the concentration of Ag nuclei in the emulsion used ($\rho = 1.01 \times 10^{22}$ atoms/cm^3) and f is the weight factor of Ag nuclei ($f = 0.62$). On the other hand, the nuclear fragmentation cross section σ_{NUC} corresponding to the charge-changing cross section is calculated from $\sigma_{NUC} = 1/n_{em}\,\lambda_{NUC}$, where n_{em} is the total number of atoms in the emulsion used (see Table 1) and λ_{NUC} is the observed mean-free-path length for nuclear interactions. Table 3 presents the experimental values of σ_{EMD} for different projectiles

Fig. 3. Relationship between $\ln N(Z)$ and $\ln Z$. The continuous line represents a power-law fit Z^{τ} for charge $9 \leq Z \leq 15$.

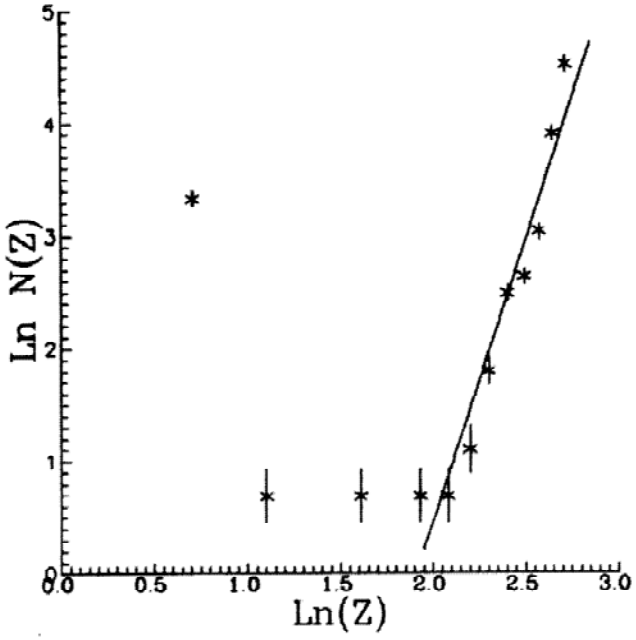

at different energies per nucleon together with the corresponding values of σ_{nuc}. From Table 3, one can see that the present value for σ_{EMD}, namely, ^{32}S at 200A GeV, agrees (within errors) with the corresponding values obtained by other authors [3, 5]. Generally, there is a dependence of the value of σ_{EMD} on the projectile energy. Such dependence is more noticeable for ^{32}S at the two energies used. Also, the dependence of σ_{EMD} on the projectile mass is only observable at ultrarelativistic energy, i.e., in the case of σ_{EMD} for ^{16}O and ^{32}S at 200A GeV. This could be due to the fact that at low energy (3.7A GeV), the virtual-photon spectrum is not enough to clarify the effect of the mass number of the projectile on the σ_{EMD}. Our experimental value of σ_{EMD} (= 1531 ± 103 mb) for the interaction of 200A GeV ^{32}S with Ag nuclei of the emulsion is in fair agreement (within errors) with the corresponding values (1792 ± 120 mb and 1380 ± 190 mb from refs. 12 and 21, respectively) obtained using a single (Ag) target, although different detection techniques were applied. Our result at 200A GeV also agrees well with that calculated theoretically for an Ag target by Pshenichnov et al. [15] (1643 mb). This shows that a heterogeneous emulsion detector can be successfully employed to measure the EMD cross section at ultrarelativistic energies.

The various partial modes of breakup of the ^{32}S projectile due to EMD at 3.7A and 200A GeV are displayed in Table 4, together with those of ref. 3 for the 200A GeV ^{32}S beam. From Table 4, it can be seen that the most prominent modes of breakup for 3.7A GeV are (in descending order) Si + He, P + p, Si + 2p, Al + He + p, and Mg + He + 2p, whereas for 200A GeV the most prominent modes are (in descending order) P + p, Si + He, Si + 2p, Al + He + p, Al + 3p, Mg + 2He, Mg + 4p, and Mg + He + 2p. Because of the low pion-producing capability of the small value of the maximum photon energy $E_{\gamma}^{\mathrm{max}}$ at 3.7A GeV, the most probable EMD channel at such energy is that having a single He

Fig. 4. Mean-free-path length λ_{EMD} of secondary 200A GeV ^{32}S PFs as a function of the charge Z in comparison with the corresponding results of ref. 5.

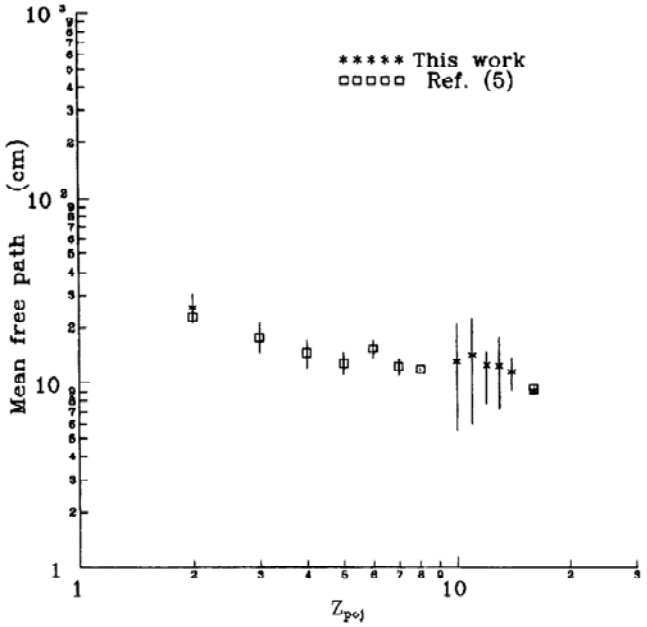

fragment. On the other hand, at 200A GeV, E_γ^{max} is quite large enough to produce protons and pions, with the consequence that the most probable EMD channel is P + p. Also, Table 4 shows the general agreement (within errors) of the present partial cross sections for the different channels with those of ref. 3 at 200A GeV.

Because of the low statistics of the EMD sample at Dubna energy, we will study only the collected EMD data at CERN energy. We start by examining the growth process of fragments for the charge distribution, i.e., the increase in the number of fragments produced with increasing charge. We accordingly plot the value of $\ln N(Z)$ as a function of $\ln Z$ for the full run of data, where $N(Z)$ is the total number of projectile fragments corresponding to a given charge $2 \leq Z \leq 15$. This distribution is presented in Fig. 3. Here the high values of charge ($Z > 8$) are described by a power law Z^τ such that $\tau = 5.04 \pm 0.13$. It should be noticed that this behavior for EMD of an ultrarelativistic projectile, which was also noted in ref. 22, is reversed in the case of peripheral nuclear collisions [23], where the straight line shows an inverse power law over a limited charge range. This reversal in behaviour may be due to the difference in production mechanisms.

We next investigate in Fig. 4 the behavior of λ_{EMD} of secondary 200A GeV ^{32}S PFs having charge $Z = 2$ and $Z > 8$ as a function of Z. This investigation can be considered as an extension to the corresponding work of ref. 5, which is performed for $2 \leq Z \leq 7$. Our results fit the decreasing trend in λ_{EMD} from ^{4}He to ^{16}O to ^{32}S.

The angular distributions $dN/d\theta$ of the present proton [18] and alpha [10] fragments emitted in the EMD events of 200A GeV ^{32}S have been studied elsewhere. Because the energy and momentum of a high-energy particle cannot be determined, in this work; an estimate of the total kinetic energy E, in the projectile rest frame, of the fragments released in the interaction was made by assigning to each fragment i a mass m_i equal to the double charge of the fragment ($m_i = 2Z_i$), and a momentum per

Fig. 5. Energy spectra for the different decay modes of the present (continuous line) EMD of 200*A* GeV ^{32}S compared with the corresponding results (broken line) of ref. 5.

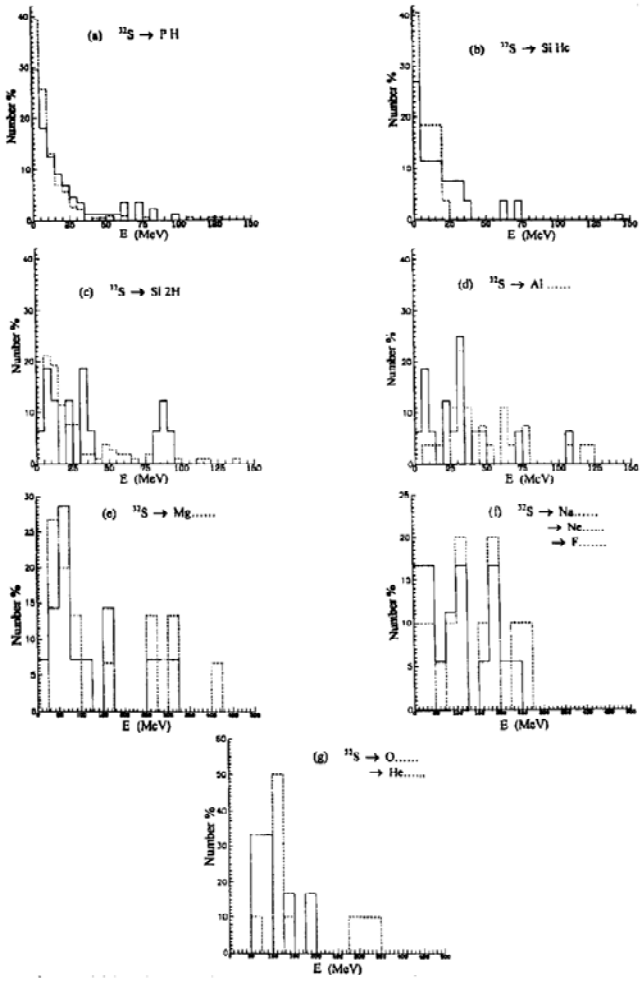

nucleon (P_i) equal to that of the incident beam. Following the rules given in ref. 5, the estimated total kinetic energy, assuming isotropy for the fragments in the projectile rest frame, is computed by the relation

$$E = \sum E_i = \frac{3}{2} \sum \frac{P_{Ti}^2}{2m_i}, \qquad p_{Ti} = p_i \theta_i$$

where the components of the transverse momentum (P_{Ti}) in the direction (θ_i) are calculated.

Table 5 shows the relative rates and numbers for the visible modes observed with 200*A* GeV ^{32}S EMD for different ranges of energy calculated using the above relation. These results are compared

Table 5. Relative rates (numbers) of the visible modes observed for 200*A* GeV ^{32}S EMD at different ranges of the released energy E. The present results are compared with similar ones calculated from ref. 5.

Channel	Energy (MeV)					
	0 – 150		> 150		> 500	
	This work	Ref. 5	This work	Ref. 5	This work	Ref. 5
P + p	53.7 ± 5.7 (88)	58.7 ± 3.7 (251)	9.1 ± 5.2 (3)	10.4 ± 4.7 (5)	7.7 ± 7.7 (1)	—
Si + 2p	9.8 ± 2.4 (16)	24.3 ± 2.4 (104)	9.1 ± 5.2 (3)	16.7 ± 5.9 (8)	7.7 ± 7.7 (1)	—
Si + He	15.8 ± 3.1 (26)	6.3 ± 1.2 (27)	9.1 ± 5.2 (3)	—	7.7 ± 7.7 (1)	—
Al + He + p Al + 3p	9.8 ± 2.4 (16)	5.8 ± 1.2 (25)	12.1 ± 6.1 (4)	14.6 ± 5.5 (7)	7.7 ± 7.7 (1)	12.5 ± 8.8 (2)
Mg + ···	5.5 ± 1.8 (9)	2.1 ± 0.7 (9)	15.2 ± 6.8 (5)	18.8 ± 6.3 (9)	—	18.8 ± 10.8 (3)
Na + ··· Ne + ··· F + ···	4.3 ± 1.6 (7)	1.2 ± 0.5 (5)	33.3 ± 10.1 (11)	20.8 ± 6.5 (10)	23.1 ± 13.3 (3)	31.3 ± 14.0 (5)
O + ··· ··· He + ···	1.2 ± 0.9 (2)	1.6 ± 0.6 (7)	12.1 ± 6.1 (4)	18.8 ± 6.3 (9)	46.2 ± 18.8 (6)	37.5 ± 15.3 (6)
Total number	164	428	33	48	13	16

with the corresponding ones of ref. 5. Figures 5*a*–5*g* show the energy spectra for the different modes displayed in Table 5. The spectra involving Al, Mg, ... as the heaviest outgoing fragments have been grouped, irrespective of the number of helium or hydrogen isotopes. From Table 5, one notices the following:

(*i*) In general, when the ultrarelativistic ^{32}S projectile decays electromagnetically into a single isotope of hydrogen (in most cases a proton) or of helium (in addition to a heavy fragment), the major contribution lies in the energy range from 0 to 150 MeV.

(*ii*) As the ^{32}S projectile decays into multifragments, the contributions in the energy ranges $E >$ 150 MeV and $E >$ 500 MeV are greater than the contribution in the range $E \leq$ 150 MeV.

From Fig. 5, one can deduce the following:

(*i*) Most of the decay modes P + p and Si + He (Figs. 5*a* and 5*b*) contribute essentially only in the giant resonance region where $E <$ 50 MeV.

(*ii*) There is a noticeable contribution of the decay mode Si + 2p in the energy range $E >$ 50 MeV, i.e., in the quasi-deuteron region, in addition to the large contribution of this mode at smaller energy (Fig. 5*c*).

(*iii*) The decay modes Al+$\cdots$ (Fig. 5*d*) mainly contribute in the energy range $E < 150$ MeV, whereas the decay mode Mg + $\cdots$ (Fig. 5*e*) extends to the energy region $E < 500$ MeV.

A general inspection of Fig. 5 shows that the corresponding energy spectra follow the same trend. However, close inspection of Fig. 5 indicates a discrepancy between the plotted spectra. Table 5 confirms the presence of such a discrepancy. In fact, the discrepancy revealed by Fig. 5 may be attributed to a difference in selection conditions for EMD events. In this work, such events are taken to be those with fragments in a narrow forward cone restricted by the condition $\theta < 1$ mrad. The value of 5 mrad, on the other hand, is used in ref. 5. The $\theta < 1$ mrad cut leads to more probable clean EMD events, as the contribution of spurious events is eliminated. These spurious events are mainly expected [5] to be due to *(i)* high-energy knock-on electrons, where the cross section tends to become zero in the very forward direction, and *(ii)* energetic electron pairs in the present selected range of photon energies, where the number of electron pairs produced per centimetre of track will vanish at the angle used [13].

5. Conclusions

In this work, the EMD of the ^{32}S projectile in nuclear emulsions is investigated at the lowest (3.7*A* GeV Dubna) and highest (200*A* GeV CERN) available energies. The results are compared with the current data for electromagnetic interactions in nuclear emulsions. We draw these conclusions:

1. At the Dubna energy, the EMD of the ^{32}S projectile represents $\approx$ 6% of the total number of detected nuclear events, whereas the corresponding value at the CERN energy represents $\approx$ 17%. These values, which agree well with those given in refs. 20 and 3, respectively, indicate the effect of the incident energy.

2. From the experimental determination of the absolute values of the overall charge-changing cross sections ($\sigma_{\mathrm{EMD}}^{\mathrm{exp}}$) for the Ag target, the following points are noticed:

   (*i*) For a single-proton (1p) emission through the channel P + p, the measured ratio $\sigma(\gamma, \mathrm{p})/\sigma_{\mathrm{EMD}}^{\mathrm{exp}}$ shows a weak energy dependence, increasing slightly from (28 ± 7)% at 3.7*A* GeV to (33 ± 3)% at 200*A* GeV. This may reflect the limiting nature of such a cross section.

   (*ii*) For a single-helium (1He) emission through the channel Si + He, the measured ratio $\sigma(\gamma, \mathrm{He})/\sigma_{\mathrm{EMD}}^{\mathrm{exp}}$ shows a reversed energy dependence, decreasing rapidly from (34 ± 9)% at 3.7*A* GeV to (11 ± 2)% at 200*A* GeV.

   (*iii*) The ratio of 1p to 1He cross sections is energy dependent. At Dubna energy, this ratio is close to unity (0.8 ± 0.2). This suggests a constant production mechanism. At CERN energy, on the other hand, the ratio rapidly increases to 3.0 ± 0.6, reflecting the dependence of the electromagnetic mechanism on projectile energy.

3. The energy released in each interaction for ^{32}S dissociation at 200*A* GeV was estimated. The energy spread indicates that most of the production of the decay channels (γ, p) and (γ, He) can be attributed to the absorption of GDRs (for $E < 50$ MeV), whereas the production of the decay channels accompanied by multifragments of hydrogen or helium can be explained in terms of multiphoton absorption [2].

4. This study is consistent with the results of Baroni et al. [5]. Moreover, the study shows the importance of electromagnetic fields generated by ultrarelativistic heavy ions, in that the cross section for EMD of nuclei becomes comparable with, or even larger than, the total nuclear cross section: $\sigma_{\mathrm{EMD}}(^{32}\mathrm{S}\text{–Ag}) \approx 1.5$ b. This means that particle production in EMD will constitute a significant background in experiments with heavy ion colliders.

Acknowledgments

The authors are grateful to the staff of the synchrophasotron at JINR, Dubna, for their help with the exposure of the emulsion stacks. They also appreciate very much the help of the authorities of CERN SPS with the irradiation of plates.

References

1. C.A. Bertulani and G. Baur. Phys. Rep. **163**, 299 (1988); Nucl. Phys. A, **442**, 739 (1985).
2. N. Ardito, G. Baroni, and V. Bisi. Europhys. Lett. **6**, 131 (1988).
3. G. Singh, K. Sengupta, and P.L. Jain. Phys. Rev. C, **41**, 999 (1990).
4. G. Singh and P.L. Jain. Z. Phys. A, **344**, 73 (1992).
5. G. Baroni, V. Bisi, A.C. Breslin et al. Nucl. Phys. **A516**, 673 (1990).
6. S.Y. Bahk, S.D. Chang, B.G. Cheon et al. Phys. Rev. C, **43**, 1410 (1991).
7. M. Nabil Yasin. Nuovo Cimento Soc. Ital. Fis. A, **108**, 1041 (1995).
8. M. Nabil Yasin, M.M. Sherif, S.M. Abd El-Halim, and M.A. Jilany. JETP, **84**, 635 (1997).
9. C.F. von Weizsäcker. Z. Phys. **88**, 612 (1934); E.J. Williams. Phys. Rev. **45**, 729 (1934).
10. (*a*) M. El-Nadi, A. Abdelsalam, A. Hussien, E.A. Shaat, N. Ali-Mossa, Z. Abou-Moussa, S. Kamel, Kh. Abdel-Waged, and M.E. Hafiz. J. Phys. G, **28**, 214 (2002); (*b*) S. Kamel. Nuovo Cimento Soc. Ital. Fis. A, **112**, 733 (1999).
11. J. Barrette, R. Bellwied, P. Braun-Munzinger et al. Phys. Rev. C, **45**, 2427 (1992); **52**, 956 (1995); V.J. Sonnadara. Nucl. Phys. **A569**, 149 (1994).
12. C. Brechtmann and W. Heinrich. Z. Phys. A, **331**, 463 (1988).
13. S. Kamel. Phys. Lett. **368B**, 291 (1996).
14. J. Barrette, P. Braun-Munzinger, W.E. Cleland et al. Phys Rev. C, **41**, 1512 (1990); W.J. Llope and P. Braun-Munzinger. Phys. Rev. C, **41**, 2644 (1990).
15. I.A. Pshenichnov, I.N. Mishustin, J.P. Bondorf, A.S. Botvina, and A.S. Iljnov. Phys. Rev. C, **57**, 1920 (1998).
16. M. El-Nadi, A. Abdelsalam, A. Hussien, E.A. Shaat, N. Ali-Mossa, Z. Abou-Moussa, S. Kamel, Kh. Abdel-Waged, and E. El-Falaky. Int. J. Mod. Phys. E, **6**, 191 (1997).
17. M. El-Nadi, A. Abdelsalam, A. Hussien et al. Nuovo Cimento Soc. Ital. Fis. A, **108**, 831 (1995); Radiat. Meas. **28**, 231 (1997).
18. S. Kamel. Nuovo Cimento Soc. Ital. Fis. A, **112**, 327 (1999).
19. B. Jakobsson and R. Kullberg. Cosmic Ray Phys. Rep. LUIP-CR-75-14. Lund. 1975.
20. D. Sampsonidis, E. Papanastassiou, M. Zamani, M. Debeauvais, J.C. Adloff, B.A. Kulakov, M.I. Krivopustov, and V.S. Butsev. Phys. Rev. C, **51**, 3304 (1995).
21. P.B. Price, R. Guoxiao, and W.T. William. Phys. Lett. **220B**, 328 (1989).
22. F.-H. Liu. Can. J. Phys. **76**, 601 (1998).
23. P.L. Jain and G. Singh. Phys. Lett. **382B**, 289 (1996).